Investigation of activation energies for dissociation of host-guest complexes in the gas phase using low-energy collision induced dissociation

Parisa Bayat, David Gatineau, Denis Lesage, Sina Marhabaie, Alexandre Martinez, Richard B Cole

Investigation of activation energies for dissociation of host-guest complexes in the gas phase using low-energy collision induced dissociation

Parisa Bayat,[a] David Gatineau,[a,b] Denis Lesage,[*a] Sina Marhabaie,[c] Alexandre Martinez,[d] Richard B. Cole[*a]

Abstract

A low-energy collision induced dissociation CID (low-energy CID) approach that can determine both activation energy and activation entropy has been used to evaluate gas-phase binding energies of host-guest (H-G) complexes of a heteroditopic hemicryptophane cage host (**Zn(II)@1**) with a series of biologically-relevant guests. In order to use this approach, preliminary calibration of the effective temperature of ions undergoing resonance excitation is required. This was accomplished by employing blackbody infrared radiative dissociation (BIRD) which allows direct measurement of activation parameters. Activation energies and pre-exponential factors were evaluated for more than 10 host-guest (H-G) complexes via the use of low-energy CID. The relatively long residence time of the ions inside the linear ion trap (maximum of 60 s) allowed the study of dissociations with rates below 1 s^{-1}. This possibility, along with the large size of the investigated ions, ensures the fulfilment of rapid energy exchange (REX) conditions, and as a consequence, accurate application of the Arrhenius equation. Compared to the BIRD technique, low-energy CID allows access to higher effective temperatures, thereby permitting one to probe more endothermic decomposition pathways. Based on the measured activation parameters, guests bearing a phosphate ($-OPO_3^{2-}$) functional group were found to bind more strongly with the encapsulating cage than those having a sulfonate ($-SO_3^-$) group; however, the latter ones make stronger bonds than those with a carboxylate ($-CO_2^-$) group. In addition, it was observed that the presence of trimethylammonium ($-N(CH_3)_3^+$) or phenyl groups in the guest's structure, improves the strength of host-guest interactions. The use of this technique is very straightforward, and it does not require any instrumental modifications. Thus, it can be applied to other H-G chemistry studies where comparison of bond dissociation energies is of paramount importance.

[a] *Sorbonne Université, CNRS, Institut Parisien de Chimie Moléculaire, IPCM, 75005 Paris, France. E-mail: richard.cole@sorbonne-universite.fr E-mail: denis.lesage@sorbonne-universite.fr*
[b] *Univ. Grenoble Alpes and CNRS, DCM (UMR 5250) BP 53, 38041 Grenoble Cedex 9 France.*
[c] *Laboratoire des Biomolécules, LBM, Département de Chimie, École Normale Supérieure, PSL University, Sorbonne Université, CNRS, 75005 Paris, France.*
[d] *Aix Marseille Université, UMR CNRS 7313-iSm2, Equipe Chirosciences, Av. Escadrille Normandie-Niemen, 13397 Marseille, France.*

Introduction

Ion-pair recognition is an intriguing area of coordination chemistry which involves the designing of receptors containing both cationic and anionic binding sites.[1–3] Cationic and anionic guests could be completely separate ions, or zwitterionic species in which the cation and the anion appear in different portions of the same molecule. The main distinction between these two situations in host-guest (H-G) chemistry is that in the case of zwitterionic species, the distance between the two binding sites in the host molecule should be matched with the size and the shape of the guest molecule.[2] This growing field of study has many applications, such as in the designing of membrane transport systems, the extraction of salts and their solubilization, and in the fabrication of sensors.[4–11] In addition, because amino acids that exist in zwitterionic form at or near physiological pH are often guests of interest, biological applications are also burgeoning.[12–15]

Various hosts have been investigated for ion-pair recognition, such as uranyl−salophen compounds,[16] or calixarene-based,[17] resorcinarene-based,[18] or pillararene-based[19] receptors. Studies of hemicryptophanes have revealed that they are also an appealing type of receptor for this purpose.[8,20–23] Hemicryptophanes are chiral molecular containers that include a cyclotriveratrylene (CTV) moiety bonded to a C_3-symmetrical organic group using three linkers whose identity and length can be varied.[24,25] Because of the heteroditopic character (i.e., tendency to simultaneously host both cationic and anionic species) of their cavity, hemicryptophanes can offer recognition properties towards ion-pairs, especially biologically important guests like taurine[20] and choline phosphate.[7]

Gas-phase investigation of host-guest systems is of great importance in providing information regarding their intrinsic structural and binding properties. Solution-phase studies have shown that hemicryptophane cages of various types can exhibit binding selectivity toward suitable guests, resulting in encapsulation of the guest.[7,8,20,21,26–28] However, the degree of encapsulation and the strength of H-G binding in solution may be influenced by solvation and counter ion effects. Gas phase studies, on the other hand, can provide a more direct means to probe intrinsic interactions between host and guest without the additional encumbrance of solvent molecules. Direct knowledge about intrinsic properties of H-G complexes achieved through gas-phase studies can

give synthetic chemists increased insight into fundamental properties of H-G systems, allowing for the improved design of cavities with refined binding properties.

H-G complexes have been subjected to various mass spectrometry-based studies with a variety of purposes such as: measurement of the energetics of H-G binding using blackbody infrared radiative dissociation (BIRD)[29],[30] or threshold collision induced dissociation (TCID),[31],[32] obtaining a relative ranking of the stabilities of H-G complexes by comparing fragmentation efficiency (or survival yield (SY)) curves,[33–35] studying the role of proton affinities of guest molecules on the characteristics of fragmentation spectra of H-G complexes,[35] exploring the structure of H-G complexes and the interactions between the two partners using the Förster resonance energy transfer (FRET) technique,[36] quantifying binding affinities by mass spectrometric titration,[37] and exploring the influence of solvent on H-G affinities.[33] These kinds of gas-phase studies, however, have been never employed for the study of hemicryptophane H-G complexes.

In using the above-mentioned techniques to investigate the energetics of H-G binding, because achievable temperatures are restricted to those accessible by resistive heating of a vacuum chamber, BIRD is limited to examining only relatively low-energy dissociations. Moreover, due to the fact that obtainment of reliable energetics in TCID requires decompositions to occur under single collision conditions, the TCID technique has been devoted primarily to the study of small systems. There are some other approaches that can be utilized to examine molecular systems having larger sizes and rather high stabilities. For example, RRKM modelling can be performed on survival yield curves obtained using a variety of collisional activation techniques such as collision induced dissociation (CID), surface induced dissociation (SID), or higher-energy collision dissociation (HCD).[38],[39] However, RRKM modelling requires information about the transition state which may not be readily accessible.

Here in this manuscript, we present a low-energy CID approach that can be used to readily determine both activation energy and activation entropy (which are related to the transition state) for dissociation of large and, at the same time, stable systems. To illustrate the advantages of the low-energy CID approach, a model system was chosen consisting of a heteroditopic hemicryptophane receptor (**Zn(II)@1**) (Figure 1) as host for some biologically-relevant guest molecules (Figure 2). Then, activation energy and pre-exponential factors of the various H-G

complexes were measured using this technique in a linear quadrupole ion trap. Because low-energy CID does not provide absolute measurements, it requires preliminary calibration of effective temperature that was achieved by employing the absolute energy measurement technique blackbody infrared radiative dissociation (BIRD)[40] on a reference H-G complex (H-G_{ref}) composed of a hemicryptophane cage as the host molecule, and betaine as the guest (Figure S1).

In the BIRD technique, ions of interest are trapped in an ultra-low pressure ($\leq 1 \times 10^{-8}$ Torr)[41],[42] Fourier transform ion cyclotron resonance (FT-ICR) mass spectrometer where they can experience unimolecular dissociation in the absence of any collisions.[43] The only source of activation is the absorption of infrared photons from the surroundings.[44],[45] In treating BIRD data, the unimolecular gas-phase ion dissociations are characterized by first-order kinetics:

$$ln\ SY = -kt \qquad (1)$$

Here, *SY* (survival yield) is the fraction of the molecular ions that do not decompose ($SY=I_p/(I_p+\sum I_f)$, where I_p is the abundance of the precursor ion and $\sum I_f$ is the sum of the abundances of fragment ions, *k* is the dissociation rate constant, and *t* is the trapping time in the ICR cell.

The dissociation rate constants are obtained at various temperatures and the subsequent plot of *ln k* versus $1/T$ allows one to deduce the activation energy (E_a) and pre-exponential factor (A) parameters (Equation 2):

$$T_{eff} = \frac{E_a}{R}\left(\frac{1}{ln\ A - ln\ k}\right) \qquad (2)$$

For large ions, such as the reference H-G complex under study here, due to the large number of infrared active modes, the rates of absorption and emission of photons are considered to be much faster than the rate of dissociation. These conditions characterize the rapid energy exchange (REX) limit.[46] In this situation, the population of precursor ions has a chance to reach thermal equilibrium with the temperature of the surrounding walls, and therefore can be considered to have a Maxwell-Boltzmann internal energy distribution. Whether an ion fulfills the REX condition, or not, depends on its size, critical energy (E_0), the transition-state entropy, and the

experimental temperature.[46] The advantage of working at the REX limit is that the obtained Arrhenius parameters are directly equal to the characteristic activation parameters of the system.

Methodology Background

In a linear trapping quadrupole (LTQ), trapping of ions in the axial direction is achieved by applying a dc voltage to the front and back lenses of the four hyperbolic rods. In the radial direction, confinement of ions is achieved by applying radiofrequency (RF) fields to the rods. In addition, the presence of helium gas helps to reduce movement of trapped ions away from the central axis. Thanks to the long residence time of the ions inside the trap, and also to the relatively high pressure of He, a large number of collisions occur.[47] As a consequence, the ions are subjected to a considerable number of activation and de-activation steps until they reach a Maxwell-Boltzmann distribution of internal energy[47] which is characterized by an effective temperature (T_{eff}).[47–52] In this condition (absence of any excitation voltage), T_{eff} is defined by the temperature of the He bath gas which is close to the ambient temperature, as was evaluated by ion-molecule equilibrium measurements inside the LTQ.[52] During the resonant activation step (i.e., application of an AC excitation voltage with the same frequency as the secular frequency of precursor ions leading to energetic collisions with the buffer gas), the kinetic energy of the ions increases and their effective temperature exceeds their initial temperature, i.e., that of the bath gas. Goeringer and McLuckey modelled the increase in T_{eff} with single frequency resonant activation based on the kinetic theory of ion transport in gases and use of the "forced damped harmonic oscillator" model and random walk simulations.[49],[50] They concluded that after resonant excitation (in the Paul trap), in the absence of fragmentation, the population of precursor ions can still have a Maxwell-Boltzmann distribution, although its effective temperature has been shifted to higher energies.[50] This new effective temperature is a function of temperature and pressure of the bath gas and the resonant excitation amplitude.[50] After applying an excitation voltage, the size of the ions will strongly influence whether the new internal energy distribution remains Maxwell-Boltzmann or not.[48] As the molecular size increases, the probability of being under rapid energy exchange (REX)[46] conditions also rises (i.e., the rates of the activation and deactivation steps far exceed the rate of dissociation).[48] Thus, for larger ions, the REX limit is easier to achieve, and under these conditions, there is less deviation from a Maxwell-Boltzmann distribution.[48] It is worth noting here that the REX limit

was first defined for activation by infrared photons performed at very low pressure conditions in BIRD experiments.[40] In BIRD experiments, at the REX limit, the rates of photon absorption/emission far exceed the unimolecular dissociation rate, and the precursor ion population arrives at a thermal equilibrium with its surrounding temperature *T*.

In the ion trap, owing to the presence of helium at relatively high pressure, the REX limit is expected to be achieved more rapidly due to the faster energy exchange by collisional activation. Furthermore, compared to the BIRD technique, higher effective temperatures can be attained, and smaller precursor ions could reach the thermal equilibrium condition.[53–55] Goeringer *et al.* tried to experimentally determine the relationship between the effective temperature and excitation amplitude by measuring dissociation rate constants (*k*) of protonated leucine enkephalin at different excitation amplitudes, and separately, at different temperatures of the bath gas.[48] They found a linear relationship between T_{eff} and excitation amplitude. In their experiment, because of the rather high dissociation rates (up to 65 s^{-1}) observed under resonant activation conditions, direct application of the Arrhenius equation was impossible.[48] Subsequently, Gabelica *et al.* attempted to perform a general calibration of effective temperature, and experimentally derive an equation that relates T_{eff} to excitation amplitude for different sizes of peptide precursor ions in the temperature range of 365 to 600 K.[56] In order to fulfil the REX condition, they worked in the regime of relatively low dissociation rates (0.01 to 5 s^{-1}). Their study found that in the above-mentioned temperature range, effective temperature is a linear function of excitation amplitude. They explained that, according to the theoretically obtained equation,[49],[50] this relation should formally be quadratic. However, they argued that, in the limited temperature range (365-600 K), approximating a linear dependence between T_{eff} and excitation amplitude also has validity.[56]

Here we employ a method for estimation of effective temperature of ions undergoing resonant excitation inside a linear ion trap which is based on the work of Goeringer and McLuckey.[49],[50] They extracted an equation describing the effective temperature of the ions activated by dipolar-single frequency resonant excitation, inside the Paul trap as follows:

$$T_{eff} = T_{bath} + \frac{m_{gas}}{6k_B(m/z)_{ion}^2}\frac{\Gamma^2 Constant^2 {V_{RF}}^2}{\xi(T_{eff})^2} \qquad (3)$$

in which T_{bath} is the temperature of the bath gas, m_{gas} is the mass of the bath gas, k_B is the Boltzmann constant, $(m/z)_{ion}$ is the mass-to-charge ratio of the ion, Γ is the compensation factor for the hyperbolic geometry of the electrodes, V_{RF} is the activation amplitude, *Constant* is a coefficient that allows conversion of electric field to the applied voltage given by: $E = Constant \times V_{RF}$. The parameter $\xi(T_{eff})$ is the reduced collision frequency which is a function of effective temperature, and is given by Equation 4:[57]

$$\xi(T_{eff}) = \frac{4}{3} N_{gas} \frac{\mu}{m_{ion}} \sqrt{\frac{8 k_B T_{eff}}{\pi \mu}} \Omega^{(1,1)}(T_{eff}) \qquad (4)$$

Here, m_{ion} is mass of the ion, N_{gas} is the number density of the neutral gas, μ is the reduced mass which is defined by ($\mu = m_{gas}m_{ion}/(m_{gas}+m_{ion})$) and $\Omega^{(1,1)}(T_{eff})$ represents a collision integral which depends on the ion/neutral interaction potential.[58] It should be noted that the "collision cross section" which is usually measured using ion mobility experiments, is in fact the collision integral, or more precisely, momentum transfer collision integral (the two terms are often used interchangeably).[59],[60]

By substituting Equation 4 into Equation 3, and then replacing all the constant parameters with C as follows:

$$C = \frac{3\pi\Gamma^2 Constant^2}{\left(16 N_{gas} k_B\right)^2} \qquad (5)$$

for *singly charged* ions, T_{eff} can be given by:

$$T_{eff} = T_{bath} + C \times \frac{(m_{gas} + m_{ion})}{m_{ion}} \frac{{V_{RF}}^2}{T_{eff}[\Omega^{(1,1)}(T_{eff})]^2} \qquad (6)$$

In our linear ion trap, similar to the Paul trap, precursor ions are excited by applying a dipolar - resonant excitation voltage to one pair of quadrupole rods. Thus, Equations 14 to 17 in reference 49 are applicable to the LTQ as well. The differences in the geometry of LTQ and Paul trap appear in their associated *Constant* coefficient and geometry compensation factor, Γ.[49]

By assuming that $\Omega^{(1,1)}(T_{eff})$ is quite weakly dependent on temperature within a limited temperature range (this will be discussed in the Results and Discussion section), Equation 6 is a quadratic function of T_{eff} whose solution is given by:

$$T_{eff} = \frac{1}{2}\left(T_{bath} + \sqrt{(T_{bath})^2 + 4C \times \frac{(m_{gas} + m_{ion})}{m_{ion}} \frac{{V_{RF}}^2}{(\Omega^{(1,1)})^2}} \right) \quad (7)$$

It should be noted that Equation 7 is the only (acceptable) solution for Equation 6 that results in a positive value for the effective temperature. We have used Equation 7 for calibration of the T_{eff} of ions undergoing resonant excitation in a linear ion trap. To accomplish this, a reference ion with known collision integral and activation parameters is needed. Preferably, the reference ion is of similar size compared to the ions under study to lend credence to the T_{eff} calibration procedure. In the case where the reference ion is in thermal equilibrium under low-energy resonant excitation conditions, the Arrhenius equation can be used to obtain its effective temperature at different excitation voltages. In this way, the value of the constant C in Equation 7 can be obtained using a reference ion. Afterwards, with a known constant C, the effective temperatures of the other ions can be derived at different excitation amplitudes by employing Equation 7. Therefore, the only main parameters required for T_{eff} calibration are the constant C and the collision integral $\Omega^{(1,1)}$.

Methods

Sample preparation

The hemicryptophane cage, **Zn(II)@1** (Figure 1) was synthesized as described previously,[7] and its stock solution (1 mM) was made using dichloromethane. Stock solutions (1 mM) of betaine (**1**), glycine (**2**), β-alanine (**3**), 4-aminobutyric acid (**4**), 7-aminoheptanoic acid (**5**), 4-aminobenzoic acid (**7**), choline phosphate (**11**), choline (**12**) and acetylcholine (**13**) were prepared in methanol; the remaining guest molecules (i.e., phenylglycine (**6**), aminomethanesulfonic acid (**8**), taurine (**9**), and 3-amino-1-propanesulfonic acid (**10**)), were prepared as aqueous solutions. Dilution of the host and each guest molecule (1:1) in methanol (to a final concentration of 10^{-6} M for each partner) gave the final individual working solutions.

A reference H-G complex (Figure S1) was selected for calibration of the effective temperature. This complex is in fact [reference cage+betaine+H]$^+$, but for simplicity, throughout this manuscript, it is called H-$G_{ref.}$ In this case, the host cage (Figure S1) was synthesized as explained previously,[7] and its stock solution (1 mM) was made using dichloromethane. A working solution of H-G_{ref} was prepared by dilution of stock solutions of the cage and betaine (1:1) in methanol (to a final concentration of 10^{-6} M for each partner).

Leucine enkephalin was purchased from Sigma-Aldrich (Taufkirchen, Germany) and its stock solution (1 mM) was made in methanol. A working solution of leucine enkephalin was prepared by diluting the stock solution to the final concentration of 10^{-6} M in methanol.

Low-energy CID experiments

Mass spectrometry experiments were conducted using a linear trapping quadrupole (LTQ)-XL/Orbitrap hybrid instrument (Thermo Fisher®, San Jose, CA). Solutions were injected into the ion source at 5 µL/min using a syringe pump. An electrospray voltage of 3.8 kV, capillary voltage of 50 V, and tube lens offset of 90 V were employed. The drying gas temperature was 275 °C, and sheath, auxiliary and sweep gas flows (all were nitrogen) of 35, 0 and 2, respectively (arbitrary units), were utilized.

Low-energy CID experiments were performed using the LTQ ion trap of the instrument. Precursor ions of interest were isolated in the LTQ prior to decomposition with an isolation window of 10 u. For these experiments, the normalized collision energy (NCE) option was disabled, and instead, peak-to-peak excitation voltage (V_{RF}) was used. Helium was used as trapping and collision gas, and the trapping parameter (q) was set at 0.25. In the case of choline phosphate where a consecutive fragmentation is observed, for the first step of dissociation, the isolation window was set at 10 u, and for the second step, it was set at 100 u to avoid any excitation of ions due to the applied waveform employed for isolation. For each resonant activation voltage, CID spectra were recorded at different activation times (30 ms - 60 s); all acquisitions were averaged to obtain the final spectrum over a 3 min data collection period. For each ion, only the intensity of the monoisotopic peak was considered.

BIRD experiments

BIRD experiments were performed using a 7T hybrid quadrupole-FTICR mass spectrometer (ApexQe, Bruker Daltonics, Billerica, USA). H-G solutions were infused at a flow rate of 120 μLh^{-1} into an Apollo II electrospray ionization source with N_2 as nebulizing gas. The temperature of the source was set at 250 °C, ESI voltage at 4500 V, capillary exit at 300 V, skimmer I at 150 V, skimmer II at 8 V. Heating of the FTICR cell for BIRD experiments was performed by installing a resistive heating metallic "ribbon" external to the vacuum system that covers the entire vicinity of the cell; applying a variable voltage to the metallic ribbon allows temperature control. A cell temperature accuracy check was performed by observing the dissociation of the sodium-bound dimer of leucine enkephalin, $(LEK_2Na)^+$, with well-known kinetic parameters, inside the cell.[61] A temperature probe, placed between the metallic ribbon and cell housing, shows a maximum temperature difference of 3 °C compared to the temperature obtained by calibration. All mass spectra were acquired using XMASS (version 6.1, Bruker Daltonics) in broadband mode. The number of data points was set at 512 K, and the time allowed for the unimolecular dissociation reaction to occur was varied by changing the "pumping delay" (without gas introduction, this corresponds to the period of time that ions are trapped in the cell).

Ion mobility experiments

Ion mobility experiments were performed using a trapped ion mobility mass spectrometry (TIMS) instrument (Bruker Daltonics, Bremen, Germany). Solutions were injected at a flow rate of 5 µL/min into an electrospray ionization source operating in the positive ion mode. Capillary voltage was set at 3.6 kV, end plate offset at 500 V, and nebulizer gas pressure at 4.4 psi. The drying gas temperature was set at 200 °C, and its flow rate at 3 L/min. Nitrogen was used as buffer gas at a temperature of 300 K. Separations were first performed in a long inverse reduced mobility ($1/K_0$) range (0.77 to 1.93 $V.s/cm^2$), and then, depending on the position of the ions of interest on the ($1/K_0$) axis, the spectra were recorded again in a decreased inverse mobility range. Accumulation time for a single analysis was set at 10 ms and the spectra were recorded for 1 min. Calibration of the inverse reduced mobility ($1/K_0$) axis was performed using Agilent tune mix (Agilent Technologies, Santa Clara, Ca, USA) and collision cross sections (CCSs) were calculated by the Compass Mobility Calculator (version 2.0) using the experimental $1/K_0$ values.

Results and discussion

Zinc metal coordination with negatively charged ligands, and the simultaneous possibility for cation-π interactions, make the **Zn(II)@1** host molecule (Figure 1) a promising receptor for ion-pair recognition. To systematically investigate the hosting capabilities of **Zn(II)@1**, a series of guest molecules with varying cationic, anionic, and linker portions (Figure 2) were selected for study. Separate solutions containing the **Zn(II)@1** host with each of the thirteen guest molecules were prepared individually as 1:1 mixtures. Positive ion mode ESI-MS spectra of these 1:1 (H:G) mixtures revealed that, with Zn(II) initially present, the majority of the complexes had undergone deprotonation to form the singly charged species. Two notable exceptions, however, were the cases of acetylcholine (13), where the H-G complex was not observed in the gas phase, and choline (12), where the singly charged H-G complex was observed, but with two additional chloride anions (or one chloride plus loss of a proton). For choline phosphate (**11**) with one negative charge, the singly charged H-G pair was detected. These observations are in keeping with the heteroditopic property of the hemicryptophane cage **Zn(II)@1**. Two example electrospray mass spectra are shown in Figure S2.

The first tandem mass spectrometry experiments attempted were BIRD experiments on the eleven H-G complexes. None of the complexes, however, were able to decompose within the accessible temperature range of our BIRD set-up (300 to 410 K). It should be noted that 410 K is the maximum value of our heating system, and even if it were possible to go higher, a further increase of the temperature would risk damage to the pre-amplifier located near the ICR cell. It is thus not possible to observe BIRD decompositions of the H-G complexes in our apparatus. Due to this constraint, the low-energy CID technique was selected to measure the bonding strengths of the various H-G pairs. In order to use this technique, the first step is calibration of the effective temperature of the ions during resonant excitation by exploiting Equation 7. For this purpose, a reference H-G complex ($H\text{-}G_{ref}$) was selected that is characterized by a structure (Figure S1) and a number of degrees of freedom (DOF) very similar to those of the H-G complexes under study. Fortuitously, the activation energy and pre-exponential factor of this H-G complex could be measured using BIRD, as decompositions were sufficiently abundant below 410 K, leading to its selection as the reference.

BIRD to determine activation energy and pre-exponential factor of reference compound

Figure 3a displays the kinetic plots for the dissociation of H-G_{ref} at different temperatures. In Figure 3b, the corresponding Arrhenius plot is shown. As is evident from Figure 3, extremely linear plots (kinetic and Arrhenius) are obtained. The activation energy (E_a) of 1.27 ± 0.05 eV and the logarithm of the pre-exponential factor (*log A*) of 14.2 ± 0.6 can be deduced from the slope and intercept, respectively, of the Arrhenius plot. According to Price and Williams,[46] for a peptide ion with *log A* of 14.5 and E_0 of 1.2 eV, the minimum molecular weight of the ion should be 787 Da to be considered as satisfying the REX limit requirements. Thus, H-G_{ref}, at *m*/*z* 1068, number of DOF of 462, E_a of 1.27 (±0.05) eV and *log A* of 14.2 (±0.6) is anticipated to readily fulfill the REX limit condition.

Low-energy CID

The low-energy CID technique requires that the selected reference H-G complex have only a single dissociation pathway. This avoids difficulties that may arise from different competitive decomposition pathways taking precedence in different dissociation time-windows (which consequently influence derived activation parameters). Therefore, it is necessary to use a reference system with a unique dissociation route, such as H-G_{ref}. Furthermore, in low-energy CID experiments, the probability of consecutive fragmentation is very low due to the resonant excitation of only the precursor ion and not the fragments, and to the very low amount of energy deposited on precursor ions, resulting in the production of fragment ions that do not have enough energy to undergo dissociation. By obtaining fragmentation efficiency curves at different times and energies, one can ensure the absence of consecutive fragmentation, and finally obtain the activation parameters for individual dissociation pathways.

After obtaining the activation parameters for the reference H-G system, temperature calibration was performed as follows: first, for H-G_{ref}, dissociation rate constants at various amplitudes (1.2 to 1.6 V) were measured (Figure 4). Relatively low dissociation rates (0.01 to 0.35 s^{-1}) were observed inside the LTQ, again strongly suggesting that the REX limit condition is fulfilled, and consequently, the Arrhenius equation (Equation 2) can be appropriately applied to calculate the effective temperature of H-G_{ref} ions at each excitation amplitude.

In addition to the V_{RF} and its corresponding T_{eff}, we need the collision integral $\Omega^{(1,1)}$ of the reference H-G complex in order to derive the constant C in Equation 7. For this purpose, ion mobility mass spectrometry was employed.

The measured value for $\Omega^{(1,1)}$ can vary depending on the employed buffer gas in the ion mobility mass spectrometer. Low-energy CID experiments were performed using helium as collision gas, therefore, ideally, collision integrals should be measured by an ion mobility mass spectrometer that uses He. However, our employed TIMS instrument is designed for use with nitrogen as the buffer gas (Experimental N_2-based collision integrals are presented in Table S1). The proportionality between He-based and N_2-based collision integrals depends on the chemical nature of the ions, and their difference is more pronounced for small ions.[59] Therefore, it can be expected that this proportionality holds for H-G complexes in this study, with very similar chemical nature, and quite large size. This proportionality has been previously observed[62] for various compounds that are very close in size to the H-G complexes under investigation in this study. According to the data presented in the supporting information from May *et al.*,[62] the ratio of He-based to N_2-based CCS values is almost constant (~0.75) for rather diverse types of compounds (carbohydrates, peptides and lipids). Furthermore, although it has been shown in a previous study that N_2 interactions with the metal portion of metal-containing ions can have a significant effect on drift times[63], the **Zn(II)** used in the current study is confined in a molecular cage while also interacting with a guest molecule. Thus, **Zn(II)** is only slightly exposed to interactions with the N_2 molecules and therefore, only a minimal effect on drift times is anticipated. Moreover, the ratio of the experimentally obtained N_2-based cross section, for example, for $[\mathbf{Zn(II)@1}+\mathbf{1}\text{-H}]^+$ vs. H-G_{ref}, is 1.1 according to Table S1, which is very close to the calculated He-based CCS ratio obtained using the trajectory method (1.2). This small difference in ratios has only a minor influence on the obtained activation energy. As such, N_2-based collision integrals were utilized instead of He-based ones. Afterwards, employing a bath gas temperature of 298 K,[49] the constant C was derived using H-G_{ref} (Table S2). This obtained value for the constant was subsequently used to calculate the effective temperature of the other ions at different excitation amplitudes (employing Equation 7).

For all H-G pairs, dissociation rate constants (k) were measured at various amplitudes (Equation 1), and then Arrhenius plots were obtained as $ln\ k$ versus $1/T_{eff}$ (Equation 2). The m/z, number of

DOF, fragment ion and measured N_2-based collision integrals for different H-G complexes are presented in Table S1. A typical low-energy CID spectrum along with the kinetic plot for an example H-G complex are presented in Figure 5, and the Arrhenius plots of all the complexes are presented in Figure 6. Finally, E_a and *log A* values for each H-G complex were calculated using the slope and intercept of the corresponding Arrhenius plot (Table 1). Details concerning the calculation of uncertainties are explained in the Supporting Information.

All the H-G complexes in this study dissociate in a very narrow effective temperature range, and the difference between the minimum and maximum temperature of the Arrhenius plot for each individual H-G complex is less than 64 K. In a very recent paper of Gabelica and Marklund,[59] the effect of temperature on CCS was studied, and based on their findings, it seems that our assumption (used in the Methodology Background section) that the collision integral is independent of the temperature is, in fact, very close to reality. In the context of that study, for a singly charged ion, a change of 64 K in the temperature span of 390-590 K should not result in a significant change in CCS. Furthermore, in another study,[64],[65] tabulated numerical calculations of $\Omega^{(1,1)}(T_{eff})$ for various compounds show that as T_{eff} increases, the collision integral decreases very slowly. Therefore, for a temperature range of 64 K, we consider our assumption to be reasonable.

It should be noted that the dissociation of complex **11**, [**Zn(II)@1**+**11**]$^+$, consists of two steps (Figure S3), and the activation parameters reported in Table 1 correspond to the second step of dissociation. Fragmentation of this complex will be discussed later. Parenthetically, it should be mentioned that, as a consistency check, similar experiments were performed on the sodium bound dimer of leucine enkephalin $(LEK_2Na)^+$ with *m*/*z* of 1133.5 and number of DOF of 459, and its Arrhenius plot is included in Figure 6. The reason for selection of $(LEK_2Na)^+$ as a reference compound is that it has a single dissociation pathway and therefore its pre-exponential factor obtained using BIRD or low-energy CID utilizing different time windows and amounts of internal energy deposition can be conveniently compared. Furthermore, in order to be cautious, it was preferred to use a system with a size quite similar to our employed H-G complexes. Because $(LEK_2Na)^+$ has almost the same cross-section as those of the H-G complexes, it was a good candidate for comparison purposes. Measured activation parameters: E_a = 1.61 ± 0.10 eV and *log*

A = 16.7 ± 1.5 are close to published values for $(LEK_2Na)^+$ obtained using the BIRD technique (E_a = 1.46 ± 0.07 eV and *log A* = 16.7 ± 0.9).[61]

Comparison of H-G complexes for various guests

The pre-exponential factors obtained using low-energy CID experiments in the LTQ are very similar for all the H-G complexes (an average of 14.6). Therefore, for comparing their stabilities, one can directly rank their activation energies. In addition, it can be expected that dissociation of all the complexes is occurring with almost the same type of rather "loose" transition state (i.e., a high value of the activation entropy (usually *log A* > 14),[40] is characteristic of direct bond cleavage from a transition state whose structure resembles those of the fragments (late transition state) with a negligible reverse activation barrier).

A closer look at the series of guests bearing a carboxylate function (Table 1): glycine (**2**), β-alanine (**3**), 4-aminobutyric acid (**4**) and 7-aminoheptanoic acid (**5**), reveals relatively weak interactions in this group of guests. Moreover, increasing the size of the alkyl chain does not have a substantial effect on the H-G binding strength. Each guest molecule in this group is likely to exhibit similar types of interactions with the host, i.e., zinc metal coordination with the carboxylate,[7] along with possible cation-π interaction[22],[66] and hydrogen bonding.[67]

In considering the complexes of phenyl glycine (**6**) and 4-aminobenzoic acid (**7**) (Figure 2), their sizes are similar, but their main difference is the position of the ammonium and carboxylate functional groups. As can be seen in Table 1, their activation energies are almost the same, indicating that the H-G interaction in this case is only slightly influenced by the relative location of the carboxylate and the ammonium. In addition, their complexes are more stable compared to the previous group, likely due to the possibility for π-π interactions between the phenyl groups of these two guests and the linkers in the cage structure.

In considering betaine (**1**) versus glycine (**2**) (Figure 2), these two molecules differ only by the presence of a trimethylammonium group (-$\mathbf{N(CH_3)_3^+}$) on the former, instead of an ammonium group (-$\mathbf{NH_3^+}$) on the latter. The main interactions that methyl groups of betaine (**1**) could participate in are C-H…π interactions with the host, and the contribution of this interaction results in a distinction between **1** and **2**, because the trimethylammonium moiety clearly augments the host-guest interaction.

In comparing the three guests bearing a sulfonate group (Figure 2), only the length of the alkyl chain separating the sulfonate function from the ammonium group is changing. It can be seen that complexes of taurine (**9**) and 3-amino-1-propane-sulfonic (**10**) acid have higher binding energies compared to that of the shortest chain aminomethanesulfonic acid (**8**). With the sulfonate group tethered to the **Zn(II)**, this result suggests the importance of the ammonium position to participate in H-G stabilization and increase interaction with the host.

For all of the guests in this study, deprotonated H-G complexes (+1 charge state) are formed in the gas phase except for choline phosphate (**11**) which has a net charge of -1. Guest **11**, like **1** has a 3-methylammonium group on one extreme, but unlike any other guest, it has a phosphate functional group. The higher stability of [**Zn(II)@1**+**11**]$^+$ results from substantial interactions such as coordination of the phosphate ligand to the metal, C-H…π and cation…π interactions, and hydrogen bonding. Additional evidence for this strong interaction comes from the unique fragmentation pattern of [**Zn(II)@1**+**11**]$^+$ (Figure S3). For all other H-G pairs, the only fragmentation pathway is the loss of guest molecule, but for [**Zn(II)@1**+**11**]$^+$, at low collision energy, the main fragment comes from loss of **N(CH$_3$)$_3$**. Then, at higher energies, loss of the whole guest becomes evident (Figure 7). The reported E_a value in Table 1 corresponds to the second step of dissociation. It should be noted that in deriving the activation parameters for [**Zn(II)@1**+**11-N(CH$_3$)$_3$**]$^+$, the experimental collision integral for the initial H-G pair was used, not that of H-G after loss of **N(CH$_3$)$_3$**. This inaccuracy is considered in the calculation of uncertainties for this H-G complex, and it was seen that even a deviation as large as ± 30 Å^2 does not have a substantial effect on the measured activation parameters.

The result that the binding energy of [**Zn(II)@1**+**11**]$^+$ is higher than all other guests (Table 1) is in complete accordance with what was observed previously in the solution phase (dimethyl sulfoxide containing 2% water).[7] In that study, nuclear magnetic resonance spectroscopy showed that **11** is fully encapsulated by the **Zn(II)@1** cage, and fluorescence spectroscopy showed that this guest has the highest power of quenching the fluorescence of the host.[7] These results, as well as the geometry optimization using density functional theory (DFT) for the [**Zn(II)@1**+**11**]$^+$ complex in a previously published paper,[7] allow us to classify host-guest interactions between hemicryptophane, **Zn(II)@1**, and biologically-relevant guests **1**-**11** as a function of two principal interactions. First, the anionic moiety that becomes coordinated to

Zn(II) is of primary importance to stabilize the complex, leading to the following stability trend: phosphate (**-OPO_3^{2-}**) >> sulfonate (**-SO_3^-**) > carboxylate (**-CO_2^-**) in agreement with results obtained in solution. Second, the cationic portion can have an interaction with the CTV cap of the hemicryptophane or the naphthyl linker. The ammonium moiety of guests **2**-**7** is deduced to have a very weak interaction in the host-guest complexes because no matter what the carboxylate-ammonium distance, the dissociation energy is almost the same. However, in the case of sulfonate **6**-**8,** the ammonium-sulfonate distance becomes more important to stabilize the host-guest complexes. Lastly, a pronounced feature enabling a heightened H-G interaction is the presence of trimethylammonium (**-$N(CH_3)_3^+$**) instead of ammonium (**NH_3^+**). Even so, this interaction remains less important than ligand-metal coordination.

Conclusions

A low-energy CID technique was implemented to investigate H-G energetics of a host hemicryptophane with heteroditopic character that is potentially useful in ion-pair recognition. This low-energy CID approach, that included kinetic experiments in a LTQ, permitted the derivation of activation parameters of various H-G complexes of **Zn(II)@1**. The relatively large residence time of the ions inside the linear ion trap (maximum of 60 s) allowed studying reactions with rates less than 1 s^{-1}. This possibility, as well as the large size of the ions, ensures the fulfillment of rapid energy exchange conditions, and as a consequence, accurate application of the Arrhenius equation. From another point of view, owing to the collisional activation occurring, even smaller systems can fulfill the rapid energy exchange conditions compared to the BIRD technique. Another contrast with the BIRD technique is that low-energy CID offers access to the higher effective temperatures required to probe more endothermic decomposition pathways. As a result, it was possible to measure activation parameters for H-G complexes that were not sufficiently fragile to undergo fragmentation within the practical (limited) upper temperature range of our BIRD set-up. Lastly, this method is much faster to implement than the BIRD technique and does not require any instrumental modifications.

Based on the measured activation energies, and considering the fact that all complexes were characterized by similar pre-exponential factors, the contribution of various functional groups to the final stabilities of H-G complexes can be ranked: guests bearing a phosphate (**-OPO_3^{2-}**) functional group make stronger interactions with the encapsulating cage than those with a

sulfonate (**-SO_3^-**) group, and the latter ones make stronger bonds than those with a carboxylate (**-CO_2^-**) group. In addition, we showed evidence that the presence of **-$N(CH_3)_3^+$** or phenyl groups in the guest's structure, improves the strength of host-guest interactions.

In summary, low-energy CID has been used to compare a series of H-G complexes with similar size and chemical nature that were dissociating in a limited temperature range (390-590 K). Due to its simplicity and wider energy range of applicability, low-energy CID can be a convenient alternative technique to other existing methods for studying the energetics of ion dissociation in the gas phase.

Conflicts of interest

There are no conflicts to declare.

Acknowledgements

The authors thank Dr. Gérard Bolbach for critical reading of, and thoughtful suggestions for, this paper. We are grateful for financial support obtained for PB from a Bourse Ministérielle (France). Financial support from the National FT-ICR network (FR 3624 CNRS) and the MetaboHUB, ANR-11-INBS-0010 grant for conducting this research are also gratefully acknowledged.

References

[1] I. O. Sutherland. Synthetic ditopic receptors. *J. Incl. Phenom. Macrocycl. Chem.* **2001**, *41*, 69.

[2] A. J. McConnell, P. D. Beer. Heteroditopic receptors for ion-pair recognition. *Angew. Chemie - Int. Ed.* **2012**, *51*, 5052.

[3] S. K. Kim, J. L. Sessler. Ion pair receptors. *Chem. Soc. Rev.* **2010**, *39*, 3784.

[4] A. C. Tagne Kuate, M. M. Naseer, K. Jurkschat. Liquid membrane transport of potassium fluoride by the organotin-based ditopic host Ph_2FSnCH_2 SnFPh-CH_2-[19]-crown-6. *Chem. Commun.* **2017**, *53*, 2013.

[5] K. Ziach, M. Karbarz, J. Romański. Cooperative binding and extraction of sodium nitrite by a ditopic receptor incorporated into a polymeric resin. *Dalt. Trans.* **2016**, *45*, 11639.

[6] P. Webber, P. D. Beer. Ion-pair recognition by a ditopic calix[4]semitube receptor. *Dalt. Trans.* **2003**, *0*, 2249.

[7] Z. Dawei, G. Gao, L. Guy, V. Robert, J.-P. Dutasta, A. Martinez. A fluorescent heteroditopic hemicryptophane cage for the selective recognition of choline phosphate. *Chem. Commun.* **2015**, *51*, 2679.

[8] J. R. Cochrane, A. Schmitt, U. Wille, C. a Hutton. Synthesis of cyclic peptide hemicryptophanes: enantioselective recognition of a chiral zwitterionic guest. *Chem. Commun. (Camb).* **2013**, *49*, 8504.

[9] F. Temel, M. Tabakci. Calix[4]arene coated QCM sensors for detection of VOC emissions: Methylene chloride sensing studies. *Talanta* **2016**, *153*, 221.

[10] S. K. Kim, J. L. Sessler. Calix[4]pyrrole-based ion pair receptors. *Acc. Chem. Res.* **2014**, *47*, 2525.

[11] P. Molina, A. Tárraga, M. Alfonso. Ferrocene-based multichannel ion-pair recognition receptors. *Dalt. Trans.* **2014**, *43*, 18.

[12] L. de Juan Fernández, Á. L. Fuentes de Arriba, L. M. Monleón, O. H. Rubio, V. Alcázar Montero, L. S. Rubio, J. R. Morán. An Enantioselective benzofuran-based receptor for dinitrobenzoyl-substituted amino acids. *European J. Org. Chem.* **2016**, *2016*, 1541.

[13] H. Huang, R. Nandhakumar, M. Choi, Z. Su, K. M. Kim. Enantioselective liquid–liquid extractions of underivatized general amino acids with a chiral ketone extractant. *J. Am. Chem. Soc.* **2013**, *135*, 2653.

[14] F. G. Herrero, O. H. Rubio, L. M. Monleón, Á. L. Fuentes de Arriba, L. S. Rubio, J. R. Morán. A molecular receptor for zwitterionic phenylalanine. *Org. Biomol. Chem.* **2016**, *14*, 3906.

[15] O. H. Rubio, R. Taouil, F. M. Muñiz, L. M. Monleón, L. Simón, F. Sanz, J. R. Morán. A molecular receptor selective for zwitterionic alanine. *Org. Biomol. Chem.* **2017**, *15*, 477.

[16] M. Cametti, M. Nissinen, A. Dalla Cort, L. Mandolini, K. Rissanen. Ion pair recognition

of quaternary ammonium and iminium salts by uranyl-salophen compounds in solution and in the solid state. *J. Am. Chem. Soc.* **2007**, *129*, 3641.

[17] M. D. Lankshear, I. M. Dudley, K.-M. Chan, P. D. Beer. Tuning the strength and selectivity of ion-pair recognition using heteroditopic calix[4]arene-based receptors. *New J. Chem.* **2007**, *31*, 684.

[18] N. K. Beyeh, D. P. Weimann, L. Kaufmann, C. A. Schalley, K. Rissanen. Ion-pair recognition of tetramethylammonium salts by halogenated resorcinarenes. *Chem. - A Eur. J.* **2012**, *18*, 5552.

[19] M. Ni, Y. Guan, L. Wu, C. Deng, X. Hu, J. Jiang, C. Lin, L. Wang. Improved recognition of alkylammonium salts by ion pair recognition based on a novel heteroditopic pillar[5]arene receptor. *Tetrahedron Lett.* **2012**, *53*, 6409.

[20] O. Perraud, V. Robert, A. Martinez, J.-P. Dutasta. A designed cavity for zwitterionic species: selective recognition of taurine in aqueous media. *Chem. - A Eur. J.* **2011**, *17*, 13405.

[21] O. Perraud, V. Robert, A. Martinez, J. P. Dutasta. The cooperative effect in ion-pair recognition by a ditopic hemicryptophane host. *Chem. - A Eur. J.* **2011**, *17*, 4177.

[22] O. Perraud, V. Robert, H. Gornitzka, A. Martinez, J. P. Dutasta. Combined cation–π and anion–π interactions for zwitterion recognition. *Angew. Chemie - Int. Ed.* **2012**, *51*, 504.

[23] D. Zhang, A. Martinez, J.-P. Dutasta. Emergence of hemicryptophanes: from synthesis to applications for recognition, molecular machines, and supramolecular catalysis. *Chem. Rev.* **2017**, *117*, 4900.

[24] V. Schurig. *Differentiation of enantiomers I*. Springer, **2013**.

[25] T. Brotin, J.-P. Dutasta. Cryptophanes and their complexes—present and future. *Chem. Rev.* **2009**, *109*, 88.

[26] A. Schmitt, V. Robert, J. Dutasta, A. Martinez. Synthesis of the first water-soluble hemicryptophane host: selective recognition of choline in aqueous medium. *Org. Lett.*

2014, *16*, 2374−2377.

[27] O. Perraud, S. Lefevre, V. Robert, A. Martinez, J.-P. Dutasta. Hemicryptophane host as efficient primary alkylammonium ion receptor. *Org. Biomol. Chem.* **2012**, *10*, 1056.

[28] O. Perraud, A. Martinez, J.-P. Dutasta. Exclusive enantioselective recognition of glucopyranosides by inherently chiral hemicryptophanes. *Chem. Commun. (Camb).* **2011**, *47*, 5861.

[29] E. A. L. Gillis, M. Demireva, M. G. Sarwar, M. G. Chudzinski, M. S. Taylor, E. R. Williams, T. D. Fridgen. Structure and energetics of gas phase halogen-bonding in mono-, bi-, and tri-dentate anion receptors as studied by BIRD. *Phys. Chem. Chem. Phys.* **2013**, *15*, 7638.

[30] L. Liu, D. Bagal, E. Kitova. Hydrophobic protein− ligand interactions preserved in the gas phase. *J. Am. Chem. Soc.* **2009**, *82*, 15980.

[31] P. B. Armentrout, M. T. Rodgers. Thermochemistry of non-covalent ion-molecule interactions. *Mass Spectrom.* **2013**, *2*, S0005/1.

[32] M. Rodgers, P. Armentrout. Noncovalent metal-ligand bond energies as studied by threshold collision-induced dissociation. *Mass Spectrom. Rev.* **2000**, *19*, 215.

[33] L. Wang, Y. Chai, C. Sun, D. Armstrong. Complexation of cyclofrunctans with transition metal ions studied by electrospray ionization mass spectrometry and collision-induced dissociation. *J. Mass Spectrom.* **2012**, *323–324*, 21.

[34] H. Abdoul-carime, B. Farizon, M. Farizon, J. Mulatier, J. Dutasta, H. Chermette. Solution vs. gas phase relative stability of the choline/acetylcholine cavitand complexes. *Phys. Chem. Chem. Phys.* **2015**, *17*, 4448.

[35] X. Ma, Z. Wei, X. Xiong, Y. Jiang, J. He, S. Zhang, X. Fang, X. Zhang. Gas-phase fragmentation of host–guest complexes between β-cyclodextrin and small molecules. *Talanta* **2012**, *93*, 252.

[36] Q. Duez, G. Knight, S. Daly, J. De Winter, E. Halin, L. MacAleese, R. Antoine, P.

Gerbaux, P. Dugourd. Action-FRET of β-cyclodextrin inclusion complexes. *New J. Chem.* **2017**, *41*, 1806.

[37] W. Wei, Y. Chu, R. Wang, X. He, C. Ding. Quantifying non-covalent binding affinity using mass spectrometry: A systematic study on complexes of cyclodextrins with alkali metal cations. *Rapid Commun. Mass Spectrom.* **2015**, *29*, 927.

[38] G. E. Johnson, T. Priest, J. Laskin. Size-dependent stability toward dissociation and ligand binding energies of phosphine ligated gold cluster ions. *Chem. Sci.* **2014**, *5*, 3275.

[39] P. M. and E. M. Mayer. Gas-phase binding energies for non-covalent Ab-40 peptide/small molecule complexes from CID mass spectrometry and RRKM theory. *Phys. Chem. C hem. P hys* **2011**, *13*, 5178.

[40] R. C. Dunbar. BIRD (blackbody infrared radiative dissociation): evolution, principles, and applications. *Mass Spectrom. Rev.* **2004**, *23*, 127.

[41] C.-Y. Lin, R. C. Dunbar. Zero-Pressure Thermal-radiation-Induced dissociation of tetraethylsilane cation. *J. Phys. Chem.* **1996**, *100*, 655.

[42] W. D. Price, P. D. Schnier, E. R. Williams. Binding energies of the proton-bound amino acid dimers Gly.Gly, Ala.Ala, Gly.Ala, and Lys.Lys measured by blackbody infrared radiative dissociation. *J. Phys. Chem. B* **1997**, *101*, 664.

[43] W. D. Price, P. D. Schnier, R. A. Jockusch, E. F. Strittmatter, E. R. Williams. Unimolecular reaction kinetics in the high-pressure limit without collisions. *J. Am. Chem. Soc.* **1996**, *118*, 10640.

[44] J. Perrin. Matter and light: An essay toward formulation of the mechanism of chemical reactions. *Ann Phys* **1919**, *11*, 5.

[45] J. Perrin. Radiation and chemistry. *Trans Faraday Soc* **1922**, *17*, 546.

[46] W. D. Price, E. R. Williams. Activation of Peptide ions by blackbody radiation: factors that lead to dissociation kinetics in the rapid energy exchange limit. *J. Phys. Chem. A* **1997**, *101*, 8844.

[47] S. A. McLuckey, D. E. Goeringer. Slow heating methods in tandem mass spectrometry. *J. Mass Spectrom.* **1997**, *32*, 461.

[48] D. E. Goeringer, K. G. Asano, S. A. Mcluckey. Ion internal temperature and ion trap collisional activation : protonated leucine enkephalin. *Int. J. Mass Spectrom.* **1999**, *182/183*, 275.

[49] D. E. Goeringer, S. A. McLuckey. Evolution of ion internal energy during collisional excitation in the Paul ion trap: A stochastic approach. *J. Chem. Phys.* **1996**, *104*, 2214.

[50] D. E. Goeringer, S. A. McLuckey. Kinetics of collision-induced dissociation in the Paul trap: A first-order model. *Rapid Commun. Mass Spectrom.* **1996**, *10*, 328.

[51] A. V. Tolmachev, A. N. Vilkov, B. Bogdanov, L. Păsa-Tolić, C. D. Masselon, R. D. Smith. Collisional activation of ions in RF ion traps and ion guides: The effective ion temperature treatment. *J. Am. Soc. Mass Spectrom.* **2004**, *15*, 1616.

[52] W. A. Donald, G. N. Khairallah, R. A. J. O'Hair. The effective temperature of ions stored in a linear quadrupole ion trap mass spectrometer. *J. Am. Soc. Mass Spectrom.* **2013**, *24*, 811.

[53] S. A. Mcluckey, J. M. Wells, J. L. Stephenson Jr., D. E. Goeringer. Novel quadrupole ion trap methods for characterizing the chemistry of gaseous macro-ions. *Int. J. Mass Spectrom.* **2000**, *200*, 137.

[54] D. J. Butcher, K. G. Asano, D. E. Goeringer, S. a. McLuckey. Thermal dissociation of gaseous bradykinin ions. *J. Phys. Chem. A* **1999**, *103*, 8664.

[55] K. G. Asano, D. E. Goeringer, S. A. McLuckey. Thermal dissociation in the quadrupole ion trap: ions derived from leucine enkephalin. *Int. J. Mass Spectrom.* **1999**, *185*, 207.

[56] V. Gabelica, M. Karas, E. De Pauw. Calibration of ion effective temperatures achieved by resonant activation in a quadrupole ion trap. *Anal. Chem.* **2003**, *75*, 5152.

[57] E. A. Mason, E. W. McDaniel. *Transport Properties of Ions in Gases*. Wiley-VCH Verlag GmbH & Co. KGaA, Weinheim, FRG, **1988**.

[58] C. S. Wang, G. E. Chang. Uhlenbeck, and J. de Boer. *Stud. Stat. Mech. II* **1964**.

[59] V. Gabelica, E. Marklund. Fundamentals of ion mobility spectrometry. *Curr. Opin. Chem. Biol.* **2018**, *42*, 51.

[60] V. D'Atri, M. Porrini, F. Rosu, V. Gabelica. Linking molecular models with ion mobility experiments. Illustration with a rigid nucleic acid structure. *J. Mass Spectrom.* **2015**, *50*, 711.

[61] P. D. Schnier, W. D. Price, E. F. Strittmatter, E. R. Williams. Dissociation energetics and mechanism of leucine enkephalin $(M+H)^+$ and $(2M+X)^+$ ions (X=H, Li, Na, K, and Rb) measured by blackbody infrared radiative dissociation. *J. Am. Soc. Mass Spectrom.* **1997**, *8*, 771.

[62] J. C. May, C. R. Goodwin, N. M. Lareau, K. L. Leaptrot, C. B. Morris, R. T. Kurulugama, A. Mordehai, C. Klein, W. Barry, E. Darland, G. Overney, K. Imatani, G. C. Stafford, J. C. Fjeldsted, et al. Conformational ordering of biomolecules in the gas phase: Nitrogen collision cross sections measured on a prototype high resolution drift tube ion mobility-mass spectrometer. *Anal. Chem.* **2014**, *86*, 2107.

[63] N. J. Rijs, T. Weiske, M. Schlangen, H. Schwarz. Effect of adduct formation with molecular nitrogen on the measured collisional cross sections of transition metal–1,10-phenanthroline complexes in traveling wave ion-mobility spectrometry: N_2 is not always an "inert" buffer gas. *Anal. Chem.* **2015**, *87*, 9769.

[64] E. W. McDaniel, E. A. Mason. The mobility and diffusion of ions in gases. **1973**.

[65] H. W. Ellis, R. Y. Pai, E. W. McDaniel, E. A. Mason, L. A. Viehland. Transport properties of gaseous ions over a wide energy range. *At. Data Nucl. Data Tables* **1976**, *17*, 177.

[66] D. A. Dougherty. The cation−π interaction. *Acc. Chem. Res.* **2013**, *46*, 885.

[67] E. A. Meyer, R. K. Castellano, F. Diederich. Interactions with aromatic rings in chemical and biological recognition. *Angew. Chemie - Int. Ed.* **2003**, *42*, 1210.

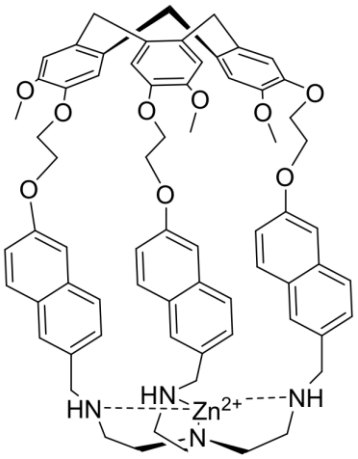

Figure 1- Hemicryptophane cage **Zn(II)@1** used as host molecule in this study.

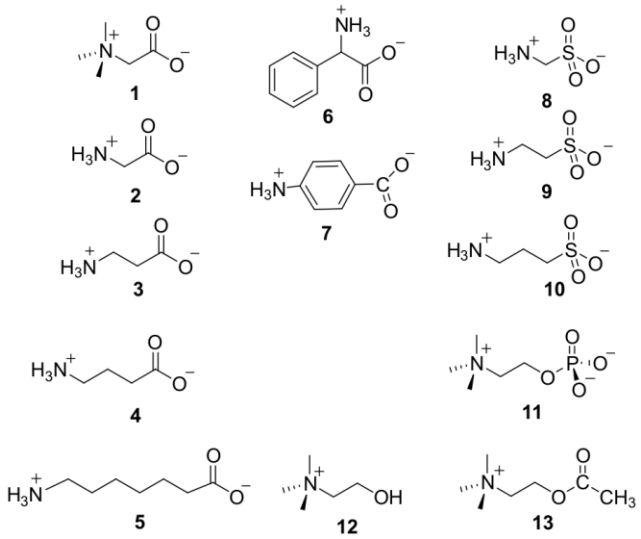

Figure 2- Guest molecules studied in this work.

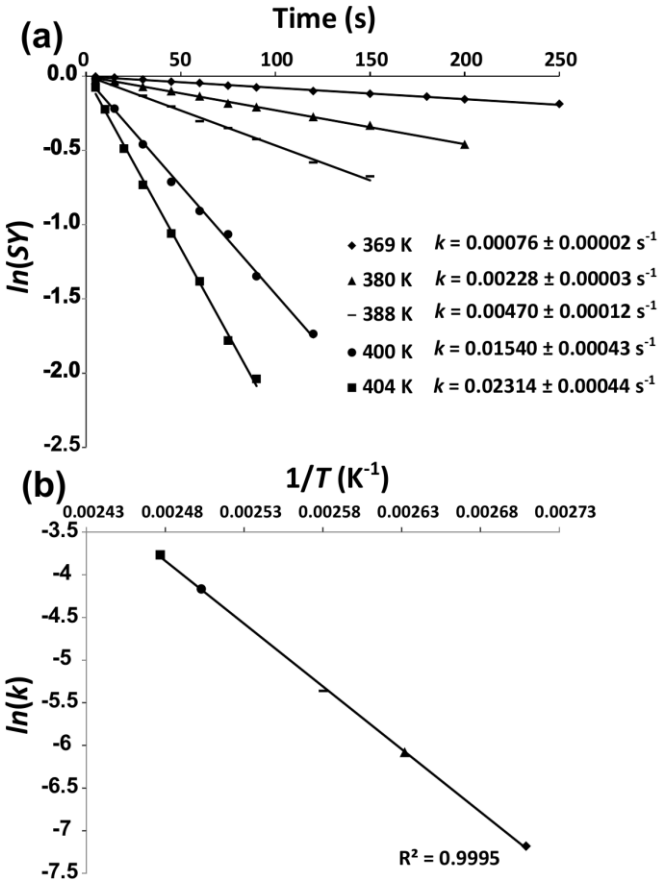

Figure 3- (a) Plots of the natural logarithm of the normalized intensity of H-G_{ref} as a function of reaction time at temperatures ranging from 369 to 404 K; (b) the corresponding Arrhenius plot for the dissociation of H-G_{ref}.

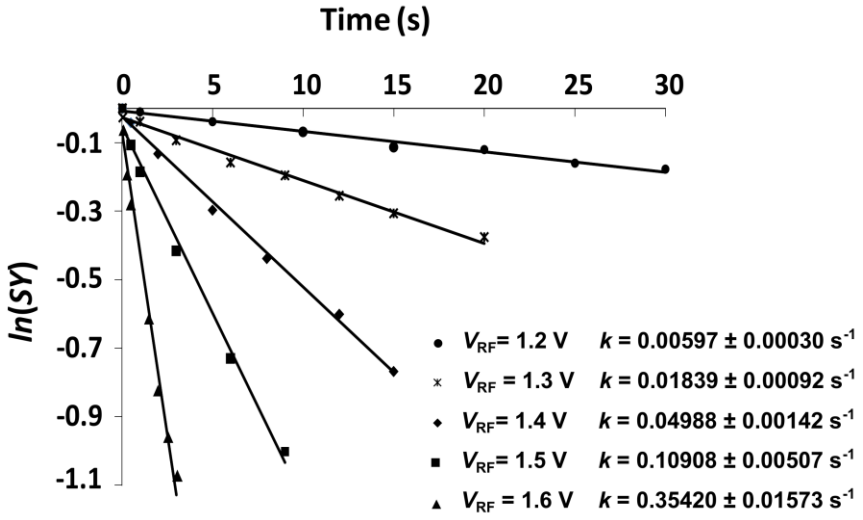

Figure 4- Kinetic plots of H-G_{ref} at different resonant activation amplitudes.

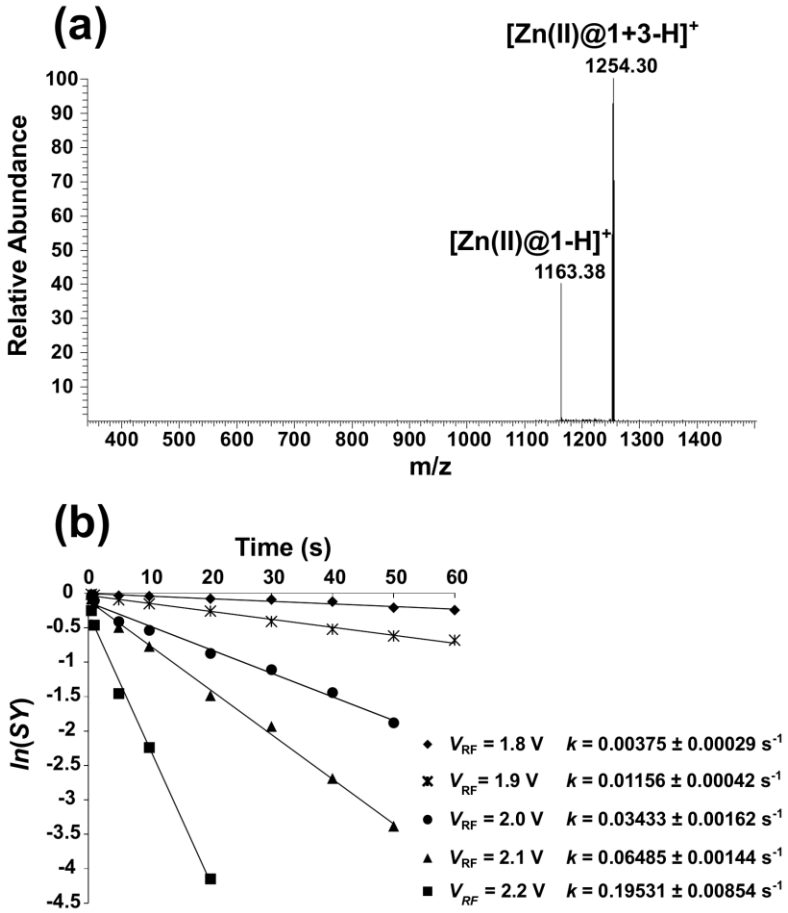

Figure 5- (a) MS/MS spectrum of the *m/z* 1252 [(**Zn(II)@1+3**)-H]$^+$ precursor obtained using low-energy CID at 1.9 V excitation voltage and 50 s decomposition time. Due to the employed resonant excitation, only the monoisotopic peak of the precursor ion (*m/z* 1252) is decomposed. (b) Kinetic plots of [(**Zn(II)@1+3**)-H]$^+$ obtained at different excitation amplitudes.

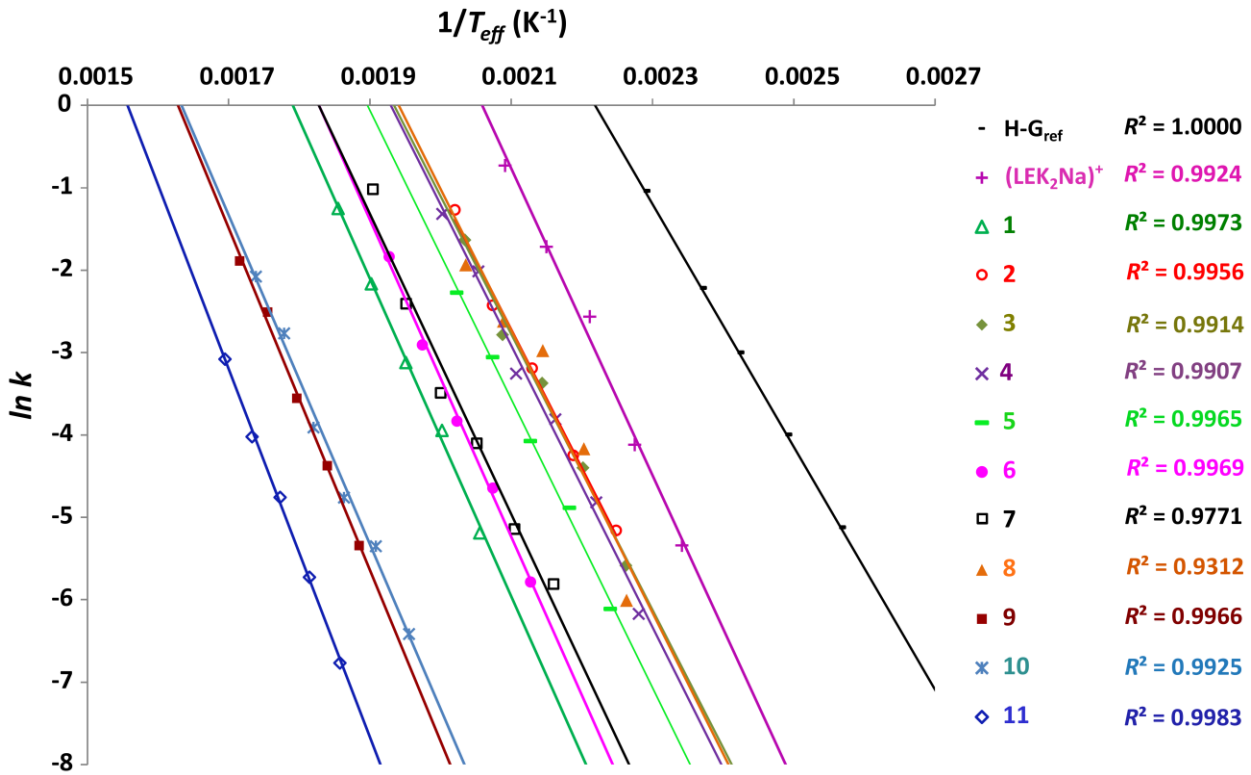

Figure 6- Experimental Arrhenius plots of the eleven H-G pairs obtained using low-energy CID. The Arrhenius plots of the reference H-G complex H-G_{ref} and $(LEK_2Na)^+$ are also displayed.

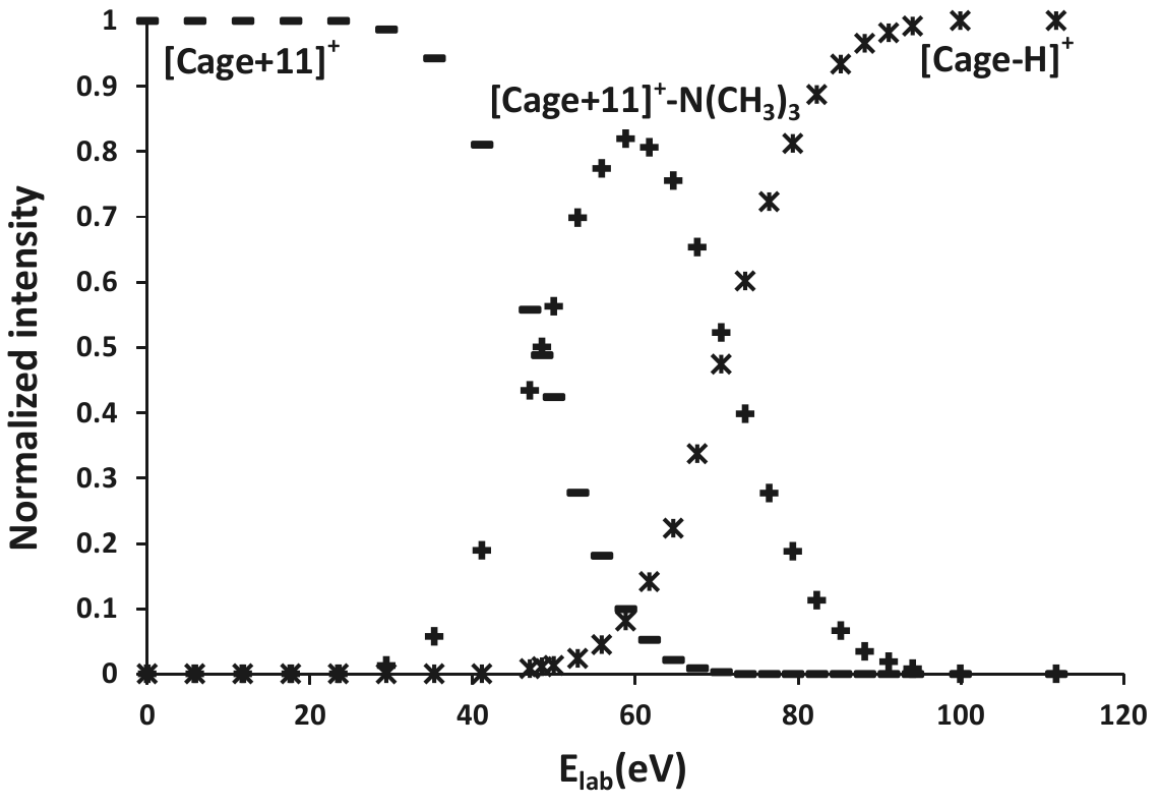

Figure 7- Normalized intensities for the [**Zn(II)@1**+**11**]$^+$ and its fragments as a function of collision energy in the laboratory frame of reference (E_{lab}), acquired using the higher-energy collision dissociation (HCD) mode of the (LTQ)-XL/Orbitrap hybrid mass spectrometer.

Table 1 Activation parameters for dissociation of Zn complexes measured by low-energy CID in the linear quadrupole ion trap.

H-G Pairs	E_a *(eV)*	*log A*
[**Zn(II)@1**+**1**-H]$^+$	1.66 (±0.08)	15.0 (±1.1)
[**Zn(II)@1**+**2**-H]$^+$	1.45 (±0.10)	14.2 (±1.2)
[**Zn(II)@1**+**3**-H]$^+$	1.44 (±0.08)	14.1 (±1.2)
[**Zn(II)@1**+**4**-H]$^+$	1.47 (±0.09)	14.3 (±1.3)
[**Zn(II)@1**+**5**-H]$^+$	1.51 (±0.08)	14.4 (±1.2)
[**Zn(II)@1**+**6**-H]$^+$	1.66 (±0.08)	15.3 (±1.2)
[**Zn(II)@1**+**7**-H]$^+$	1.57 (±0.10)	14.5 (±1.3)
[**Zn(II)@1**+**8**-H]$^+$	1.48 (±0.13)	14.4 (±1.5)
[**Zn(II)@1**+**9**-H]$^+$	1.79 (±0.06)	14.7 (±0.8)
[**Zn(II)@1**+**10**-H]$^+$	1.72 (±0.06)	14.2 (±0.9)
[**Zn(II)@1**+**11**]$^+$	1.93 (±0.11)	15.1 (±0.9)